



Use of Nuclear Medicine Molecular Neuroimaging to Model Brain Molecular Connectivity

8

Carlos A. Sanchez-Catasus, Martijn L. T. M. Müller,
Peter Paul De Deyn, Rudi A. J. O. Dierckx,
Nicolaas I. Bohnen, and Lester Melie-Garcia

C. A. Sanchez-Catasus (✉)

Division of Nuclear Medicine, Department of Radiology, University of Michigan,
Ann Arbor, MI, USA

Department of Nuclear Medicine and Molecular Imaging, University of Groningen,
University Medical Center Groningen, Groningen, The Netherlands

e-mail: carlosas@umich.edu

M. L. T. M. Müller

Division of Nuclear Medicine, Department of Radiology, University of Michigan,
Ann Arbor, MI, USA

Morris K. Udall Center of Excellence for Parkinson's Disease Research, University of
Michigan, Ann Arbor, MI, USA

e-mail: mtmuller@umich.edu

P. P. De Deyn

Department of Neurology and Alzheimer Center, University of Groningen, University
Medical Center Groningen, Groningen, The Netherlands

R. A. J. O. Dierckx

Department of Nuclear Medicine and Molecular Imaging, University of Groningen,
University Medical Center Groningen, Groningen, The Netherlands

e-mail: r.a.dierckx@umcg.nl

N. I. Bohnen

Division of Nuclear Medicine, Department of Radiology, University of Michigan,
Ann Arbor, MI, USA

Morris K. Udall Center of Excellence for Parkinson's Disease Research, University of
Michigan, Ann Arbor, MI, USA

Department of Neurology, University of Michigan, Ann Arbor, MI, USA

Neurology Service and GRECC, Veterans Administration Ann Arbor Healthcare System,
Ann Arbor, MI, USA

e-mail: nbohnen@umich.edu

© Springer Nature Switzerland AG 2021

R. A. J. O. Dierckx et al. (eds.), *PET and SPECT in Neurology*,
https://doi.org/10.1007/978-3-030-53168-3_8

181

L. Melie-Garcia

Laboratoire de Recherche en Neuroimagerie (LREN), Centre Hospitalier Universitaire
Vaudois (CHUV), Lausanne, Switzerland

Applied Signal Processing Group, Swiss Federal Institute of Technology Lausanne (EPFL),
Lausanne, Switzerland

Contents

8.1	Introduction.....	182
8.2	From Topography to Topology: The Graph Theoretical Analysis.....	184
8.3	Brain Molecular Networks: The Connectivity Matrix.....	186
8.3.1	Brain Molecular Connectivity in the Context of Structural and Functional Connectivity.....	190
8.4	Network Metrics.....	191
8.4.1	Integration.....	192
8.4.2	Segregation.....	192
8.4.3	Centrality.....	193
8.5	Brain Connectivity Analysis.....	195
8.6	Sparse Inverse Covariance Estimation (SICE).....	196
8.7	Example Studies.....	197
8.7.1	Age-Associated Metabolic Network Changes.....	197
8.7.2	Modularity of Amyloid Networks.....	199
8.7.3	Cerebrovascular Reactivity in MCI.....	200
8.7.4	SICE Application to Multimodal Neuroimaging.....	202
8.8	Final Remarks.....	202
	A Lexicon of the Most Commonly Used Network Metrics.....	204
	References.....	205

Abstract

We introduce basic concepts of brain networks and discuss methods to model and analyze brain molecular connectivity using positron emission tomography (PET) and single-photon emission computed tomography (SPECT). Basic elements of network analytic methods, including graph theory, and the connectivity matrix as a basis for network analysis will be discussed in more detail. Statistical methods to compare networks will be reviewed. A specific brain network analysis method called sparse inverse covariance estimation (SICE) is presented as an alternative to Pearson correlation to estimate the brain molecular connectivity matrix. Finally, we will discuss examples from published research to illustrate the practical application of brain molecular connectivity analysis concepts.

8.1 Introduction

This chapter will focus on the construction and analysis of brain molecular networks using nuclear medicine molecular neuroimaging. The advance of multimodal neuroimaging techniques and mathematical analysis methods has provided a great

opportunity to more comprehensively capture brain network functioning. Traditional methods of nuclear medicine molecular neuroimaging analysis have emphasized analysis based on a single or small number of brain regions. This reductionist approach of using a “process of elimination” has led to a better understanding of brain functioning. Although this method is fruitful to understand the relationship between a specific brain region and behavioral or clinical function, it generally will fail to more fully capture the wide spectrum of behavioral functions or clinical symptomatology. That is because dysfunction of one specific brain region will propagate through the larger network and will affect regions that are both directly structurally connected or indirectly functionally connected. A classic example of this is diaschisis where local dysfunction in a single brain region may cause remote deaf-ferentation effects (Monakow 1914).

In recent years there has been a growing interest in multivariate methods to analyze nuclear medicine molecular images. The first attempts to model brain networks using multivariate analysis methods were made in the last two decades of the last century by analyzing covariations of FDG-PET data (Horwitz et al. 1984; Horwitz et al. 1987; Metter et al. 1984; Clark and Stoessl 1986; Moeller et al. 1987; Eidelberg et al. 1994). For example, studies by Eidelberg et al. (1994) demonstrated the existence of specific brain metabolic covariance profiles in Parkinson disease (PD) that were associated with some of the motor and cognitive symptoms of PD (Eidelberg et al. 1994).

The dawn of the so-called connectomic era spurred mainly MR-based brain connectivity analysis (Sporns et al. 2005). Brain networks were modeled by analyzing structural connectivity using diffusion tensor images (DTI) and functional connectivity through functional magnetic resonance imaging (fMRI) as well as electroencephalography (EEG) and magnetoencephalography (MEG) (Fornito and Bullmore 2015). More recently, there is a renewed interest in brain molecular connectivity, based on molecular PET and SPECT, to define networks using radiotracers that can capture network of brain metabolism, neurotransmission, and proteinopathies among others. Many of the ideas and methods developed for the analysis of brain networks for MRI/EEG/MEG neuroimaging modalities have been gradually adapted for the analysis of brain networks based on PET and SPECT. Prevailing methods include seed-based correlation analysis (Lee et al. 2008), principal component analysis (PCA) (Manzanera et al. 2019), independent component analysis (ICA) (Gu et al. 2019), and methods based on pairwise covariance of brain regions (Yakushev et al. 2017; Sala and Perani 2019; Huang et al. 2010). The feasibility of the latter has also been shown in the analysis of cerebral blood flow (CBF) networks using SPECT (Melie-Garcia et al. 2013; Sanchez-Catasus et al. 2017; Sanchez-Catasus et al. 2018).

Perhaps due to its relative simplicity and practical feasibility, one of the most widespread methods is based on a pairwise covariance analysis of brain regions in conjunction with graph theory. This methodology allows for using metrics that capture the strength or “health” of the brain network. A specific type of the pairwise covariance approach is the sparse inverse covariance estimation (SICE) methodology that has gained recent interest (Huang et al. 2010). In this chapter, we aim to

introduce and discuss the basic elements of these methods targeting readers working in the field of neuro-nuclear medicine who may not be familiar with the underlying principles of these approaches.

Section 2 presents basic concepts of network and graph theoretical analysis. Section 3 defines the concept of the connectivity matrix which may have especially application for networks based on nuclear medicine molecular neuroimaging. In Sect. 4, frequently used network metrics are discussed in more detail. Section 5 presents the analysis of brain molecular connectivity based on the statistical comparison of metrics from at least two networks. Section 6 addresses the SICE methodology as an alternative to more standard Pearson correlation coefficient-based method. Finally, Sect. 7 will briefly discuss some recently published studies to illustrate the major concepts explained in this chapter.

8.2 From Topography to Topology: The Graph Theoretical Analysis

A key concept of graph theory is the notion of topology. Topology can be illustrated with a common network concept that one can encounter when traveling by subway in a large city. In Fig. 8.1, the left map of the London subway shows a precise spatial description of the railway (or lines) layout, i.e., the subway topography, the right map represents the relative locations of subway stations and connecting lines, i.e., the subway topology. These two maps do not coincide with regard to the relative

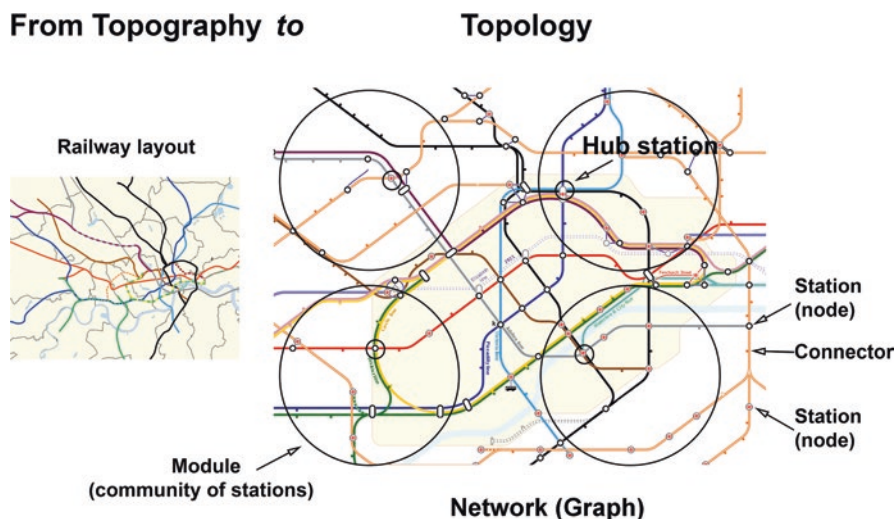


Fig. 8.1 The topographical (left) and the topological maps (right) of the London subway. Both maps are partially shown and modules (large circles) and hubs (small circles) are for illustrative purposes only. Topographical map source: https://en.wikipedia.org/wiki/File:London_Underground_with_Greater_London_map.svg. Topological map source: https://en.wikipedia.org/wiki/List_of_London_Underground_stations

position of the stations, neither in distance nor in location of lines. For example, two stations may be topographically (physically) distant but with a direct connection they can be topologically close and vice versa. The direct connection cannot be easily derived from the topographical map but is readily recognized from the topological map. The topological map is a “graph” and represents a network.

A graph is composed of two main topological elements (see also Fig. 8.1), the nodes (the stations in the subway example), and the connectors or edges (the connecting lines). While the topological map makes it easier to extract relevant information for travel on the subway, this would not be sufficient to compare the London subway with the subway of another large city, for example, to compare which subway system is more efficient. This is why quantitative measures of the network (graph) are needed. Graph theory, founded by Swiss mathematician Leonhard Euler as early as the eighteenth century (Biggs et al. 1986), is the mathematical framework for calculating these network metrics. In general, network metrics can be grouped into measures of integration, segregation, and centrality. In this section we will provide an intuitive concept of these measures. Section 4 will address these measures in more detail.

In network analysis, the concept of integration is related to communication between all the nodes of the network, i.e., how well-connected are any pair of nodes. A measure of integration in the example of the London subway would be the average number of stations that must be crossed to go from any part of the city to another; the lower the number of stations, the higher the efficiency of the subway integration.

In contrast to network integration, network segregation is related to the partition of the network into smaller graphs or a cluster of connected nodes (subgraphs). In case of the London subway graph, a natural partition is defined by taking different subgraphs formed by the stations and its direct topological neighbors. In some stations, neighboring stations are better connected than in others. For example, suppose that a particular station is out of service due to an electrical failure, if its neighboring stations are well connected to each other, it will be more easy to reroute (reconnect) the passengers to the final destination.

A more complex metric of segregation is related to what extent the whole subway can be divided into modules (i.e., groups of stations within the large circles in Fig. 8.1) in such a way that the number of connections between the stations within the module is the maximum possible while the number of connections between modules is the minimal necessary to maintain the whole subway optimally interconnected. For example, when a group of stations (module) is out of service, the remaining subway still can continue to operate due to the relative independence among modules. Therefore, a modular structure increases flexibility, stability, and robustness.

Centrality refers to the level of influence of a node on other nodes. The nodes with the highest centrality (or influence) are called hubs and are key elements in network functioning. Some nodes have a high influence on communications between modules (connector hubs), for example, the subway stations within the small circles in Fig. 8.1. Other nodes facilitate communication between the nodes that make up each module (provincial hubs). Connector hubs are crucial for network integration while provincial hubs are critical for network segregation. In Sect. 4 centrality measures are described to differentiate these two types of hubs.

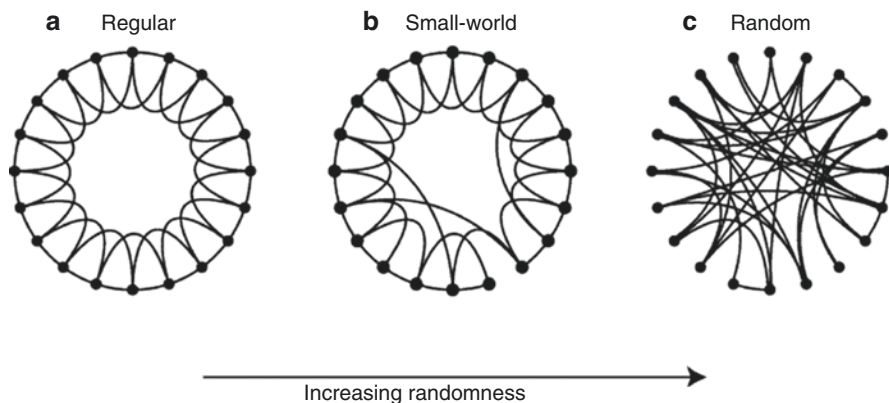


Fig. 8.2 Representation of a computational model of small-world (complex) networks which positions between regular and random networks. (Adapted from Watts and Strogatz (1998) with permission)

If networks were to be ranked, at one end of the spectrum would be a regular (ordered) network. In a regular network each node is directly connected to its neighboring nodes (short direct connection), but without direct connections to distant nodes; i.e., a network with low integration but high segregation (Fig. 8.2a). At the other end of the spectrum would be a random network. In a random network, direct connections between any two nodes are random (Fig. 8.2c); i.e., in a random network, the integration is high and the segregation is low. In the middle of these two extremes is a complex network (Fig. 8.2b), in which there is a balance between integration and segregation. A complex network has a “small-world” topology (Watts and Strogatz 1998). The concept of “small-world” comes from the social sciences and reflects the fact that two persons (nodes) who do not know each other are nevertheless connected by a relatively short chain of persons known to each other (a.k.a., the “six degrees of separation” theory).

Unlike ordered and random networks, a complex network has a modular structure and the presence of hubs (see also London subway example). These London subway concepts can be applied also to brain network analysis. Brain networks follow a “small-world” topology, with an efficient modular structure and the presence of hubs (Bullmore and Sporns 2009; Rubinov and Sporns 2010; Fornito et al. 2013). Notably, these properties remain across different spatial scales: from micro (networks of neurons) to macro (networks of brain regions).

8.3 Brain Molecular Networks: The Connectivity Matrix

We will use an example with FDG-PET to illustrate the application of network analysis to molecular imaging. Network analysis is not limited to FDG PET; the methodology described here can also be applied to PET (or SPECT) of other molecular tracers (see study examples in Sects. 8.7.2 and 8.7.3).

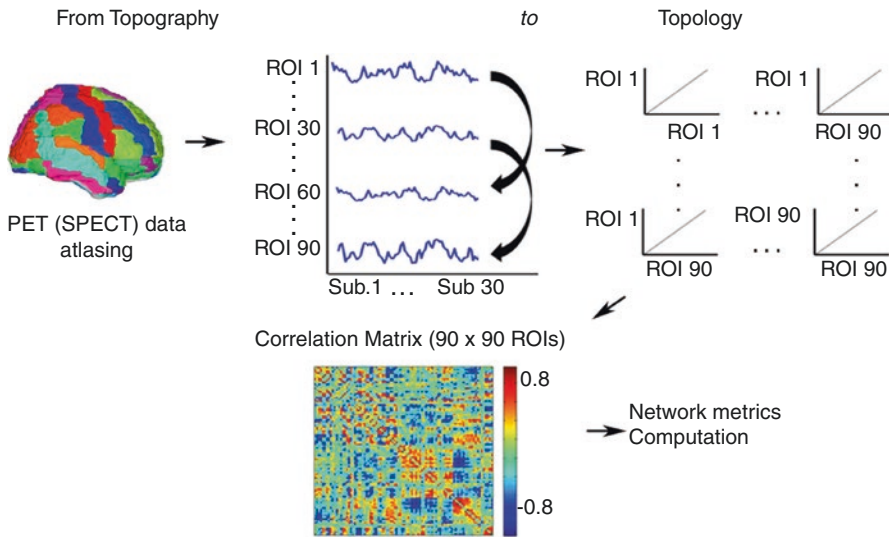


Fig. 8.3 Construction of a brain glucose metabolic network using FDG-PET data. The color bar indicates the value of the correlation coefficient coming from the brain metabolic co-variations among 90 anatomical brain regions (AAL atlas). The diagonal elements of the constructed matrix (self-correlations) are set to zero

In this example, we assume that there is a group of FDG-PET images corresponding to 30 healthy control subjects (or 30 patients with the same CNS disorder). The images of each subject can be segmented into different regions of interest (ROIs) using a brain atlas, for instance, the automated anatomical labeling (AAL) atlas (Tzourio-Mazoyer et al. 2002). If we plot the mean voxel value of each ROI for the 30 subjects, we have a measure of how each ROI varies across subjects (Fig. 8.3). Figure 8.3 shows that ROI 1 and ROI 60 (although with different amplitudes) change similarly. The same for ROIs 30 and 90. A simple way to measure how similar the variations are between any pair of ROIs across subjects is by calculating the Pearson's correlation coefficient between two different ROIs. If this process is performed for every pair of ROIs, a matrix of Pearson's correlation coefficients is obtained (Fig. 8.3).

The correlation matrix defines "the connectivity matrix," also known as the adjacency matrix, and can be seen as a network (or a graph) of interactions between all pairs of brain regions. In this example, the network nodes are the ROIs (equivalent to the subway stations) and the connectors are the Pearson correlation coefficients between any two ROIs; the FDG-PET data of a group 30 individuals have been transformed from a topographic space to a topological one (the brain glucose metabolic network). This connectivity model assumes that covariations in brain metabolism between different regions form a network.

The connectivity matrix is a basic concept of brain network analysis common to other neuroimaging modalities. For example, for DTI MRI the connectivity matrix is based on the number of tracts or streamlines connecting the ROIs, and for fMRI

the connectivity matrix is based on temporal correlations of the BOLD signal. A fundamental difference is that the connectivity matrix using PET (or SPECT) is group-based due to the “static” nature of the data while DTI and fMRI based networks can be constructed on an individual base. In recent years, however, several methods have been developed that allow the extraction of individual information from a group-based connectivity matrix (Batalle et al. 2013; Raj et al. 2010; Saggat et al. 2015; Tijms et al. 2012; Zhou et al. 2011). Other alternatives have also been proposed for single-subject level analysis (Titov et al. 2017; Tomasi et al. 2017). The development and validation of optimal methods for single-subject analysis is perhaps one of the most important research directions in the near future, since it opens the door to the use of molecular network analysis in clinical practice.

In the above FDG-PET example, the Pearson’s correlation was used. One of the problems with this statistical measure is that it estimates the association between two brain regions without considering the influence that other brain regions may have on that relationship. One way to solve the problem is to use the partial correlation measure. This requires, however, more subjects than the number of ROIs, which could be cost-prohibitive for PET or SPECT imaging studies. One possible solution is to reduce the number of ROIs, using only those that are relevant in the context of an a priori hypothesis. However, this approach has the risk that ROIs that could potentially be important may be ignored. In addition, by reducing the number of ROIs, the resulting network may not be a complex network (i.e., small-world, modularity, and the presence of hubs). Although the use of partial correlation is the optimal method to build the connectivity matrix, a recent study showed that the Pearson’s correlation is also valid to study brain molecular connectivity using radio-tracer probes, albeit with certain limitations (Veronese et al. 2019).

Another important point relates to the connectivity weights between brain regions. Connections between different neuronal units are not the same in terms of the number of synapses, axonal density, or the degree of fiber myelination. These differences can be represented by different connectivity weights between brain regions, for example, using the value of Pearson’s correlation coefficient between ROIs as shown in Fig. 8.3. Weights based on the Pearson’s correlation range from +1 (perfect positive correlation) to -1 (perfect negative correlation or anti-correlation). Many brain connectivity studies, however, rule out or ignore negative correlations, since its meaning is not entirely clear. Some network metrics also cannot be defined if negative correlations are considered. Several researchers attribute the negative correlations to statistical artifacts (Saad et al. 2012; Murphy et al. 2009; Murphy and Fox 2017), while other authors believe that negative correlations may reflect inhibition or deactivation (Anticevic et al. 2012). A possible alternative is to consider the absolute value of the resulting correlation coefficient when calculating network metrics, assuming that the relevant biological information is the presence of a statistical interaction, regardless of the correlation sign. However, the role of negative correlations will need further clarification for a better understanding in the case of brain molecular connectivity analysis.

Another important consideration is related to the extent that a given weight represents a biological connection or may be only due to noise or a spurious link.

Networks based on correlation matrices have a nonzero value in every off-diagonal element of the matrix, that is, every node is connected to every other. However, brain networks tend to be sparse by following a principle of economics, which means that the total cost of wiring in the network is less than if the same nodes were randomly connected, but at the same time maximizing the efficiency of information processing (economically connected) (Bullmore and Sporns 2012).

To address this problem, thresholds are usually applied to the correlation matrix to eliminate weights that may be due to false connections. In brain molecular imaging connectivity studies, the most used threshold method applies a global threshold to all elements of the connectivity matrix. Weights that survive the threshold are set to one (connection) and zero (no connection) otherwise, which results in a binary graph. This has the advantage that it is easier to not only characterize the network but also to make statistical comparisons (Sect. 5). The most commonly used method to define a threshold uses the concept of network density (also termed “cost” or “sparsity” in the literature). Network density represents the proportion of supra-threshold connections of all possible connections. Since threshold selection is arbitrary, the connectivity matrix is thresholded in a range of network densities instead. The area under the curve (AUC) across the threshold range is often used as the descriptor of a given network metric (Fornito et al. 2013).

A widely used criterion to choose the threshold range (both lower and upper thresholds) is based on avoiding a fragmented or fully connected network. In this case, the lower threshold is selected as the minimum network density, below which the network would be fragmented. The network is not fragmented when all its nodes are connected by an edge path, forming a single connected component. Also, as the network density decreases, it tends to be a regular network. On the other hand, to select the upper threshold, a threshold in which the network is fully connected should be avoided, as this occurs at higher densities.

Furthermore, selection of the lower and upper threshold is often dependent on the specific brain disorder and type of data used. This often will require an exploratory analysis of the data set, which will limit the use of an a priori selection. Nonetheless, the range between the upper and lower threshold moves typically from 0.1 (10% of all possible connections) to 0.5 (50%). The example in the Sect. 8.7.1 illustrates the concept of network metrics evaluation across a range of network densities.

In summary, the most common analysis of brain molecular connectivity is accomplished by using unweighted (binary) undirected graphs, that are based on Pearson’s correlation, discarding negative weights, and are only based on group-level analysis. Even with these simplifications, this method can provide important information about the molecular organization of the brain in various brain disorders. Moreover, in recent years there have been advances in the weighted graph approach and increasing calls for use across all neuroimaging modalities (Bassett and Bullmore 2017). There are also alternative methods for connectivity matrix thresholding. However, each of these thresholding methods has its own advantages and limitations. Detailed discussion of these methods is beyond the scope of this chapter but have been reviewed by Fornito et al. (Fornito et al. 2013).

8.3.1 Brain Molecular Connectivity in the Context of Structural and Functional Connectivity

Different neuroimaging modalities are proxies of different brain characteristics, e.g., DTI can be used for estimation of brain structure (principally white matter), fMRI can be used for function, and molecular imaging (PET and SPECT) for molecular activity. The information provided by these techniques allows modeling of different aspects of large-scale brain networks.

Brain structural connectivity based on DTI refers to anatomical connections between brain areas through fiber bundles. Structural connectivity is relatively stable on a short time scale (e.g., minutes) although it is subject to change on a larger time scale. In contrast, brain functional connectivity based on fMRI is related to the temporal statistical dependence between brain regions, regardless of whether these regions are connected by nerve fibers (direct structural links), with changes that can be in short periods of time (e.g., seconds). Previous studies support the notion that structural and functional connectivity are correlated (Skudlarski et al. 2008; Honey et al. 2010). If there is a strong structural connection between two brain regions, it is likely that the corresponding functional connection is also strong, although the opposite is not always true (Koch et al. 2002; Mišić et al. 2016). This is because the structural connectivity infers a direct physical or anatomical connection between any two regions, while functional connectivity incorporates direct and indirect statistical associations. In this sense, molecular-imaging based brain metabolic connectivity is more analogous to fMRI-based functional connectivity, since there could be indirect metabolic covariations (“connections”) without a specific anatomical substrate. Indeed, recent studies have shown an association between functional connectivity by fMRI and glucose metabolism derived from FDG-PET (Passow et al. 2015; Riedl et al. 2016), suggesting that the analysis of both could be complementary.

Brain molecular connectivity can also be modeled for radiotracers targeting neurotransmission systems, e.g., dopamine. In this case, the connectivity model reflects covariations of neurotransmitter binding in a given region with neurotransmitter binding in other regions (Hahn et al. 2019). Likewise, network analysis of radiotracers that visualize brain pathology (e.g., β -amyloid plaques) assumes that the pathology spreads in a network-like manner (Sepulcre et al. 2013; Pereira et al. 2018).

It is important to note that brain connectivity inferred by either DTI, fMRI, or based on molecular radiotracers does not make any explicit reference to a specific directionality, so it is not possible to estimate the causal directionality of the connectivity. This is reflected in the symmetry of the connectivity matrix (in which the upper half above the main diagonal is a mirror of the lower half) (Fig. 8.3). In these cases, the graph corresponding to the connectivity matrix is “undirected.” The so-called “effective connectivity” analysis aims to overcome this limitation through methods designed to capture the direct causal influences between brain regions (Friston 2011; David et al. 2008). More recently, a novel approach to infer effective connectivity has been suggested using the simultaneous acquisition of fMRI and FDG-PET (Riedl et al. 2016).

8.4 Network Metrics

The earlier introduced concepts of integration, segregation, and centrality metrics can be defined at a local (nodal level) and network-wide level. Figure 8.4 provides a simplification of networks to visually guide the explanation of these network metrics. Appendix A provides a lexicon of the most commonly used network metrics. Figure 8.4a shows a connectivity matrix of a hypothetical network of only 24 nodes. These nodes could be 24 London subway stations or 24 brain ROIs based on FDG-PET imaging as explained in Sects. 2 and 3, respectively. Figure 8.4b–d shows the representation of the connectivity matrix in the form of graphs displaying some simple but fundamental topological measures (shortest path, B; triad, C; and modules, D). The graph is undirected and binary, and direct connections (edges) between many pairs of nodes do not exist, although there may be indirect connections through other intermediate nodes. This is a real-life representation. For example, many stations in the London subway do not have direct connections, but are interconnected through others. Similarly, many direct edges in an FDG-PET based connectivity matrix (e.g.,

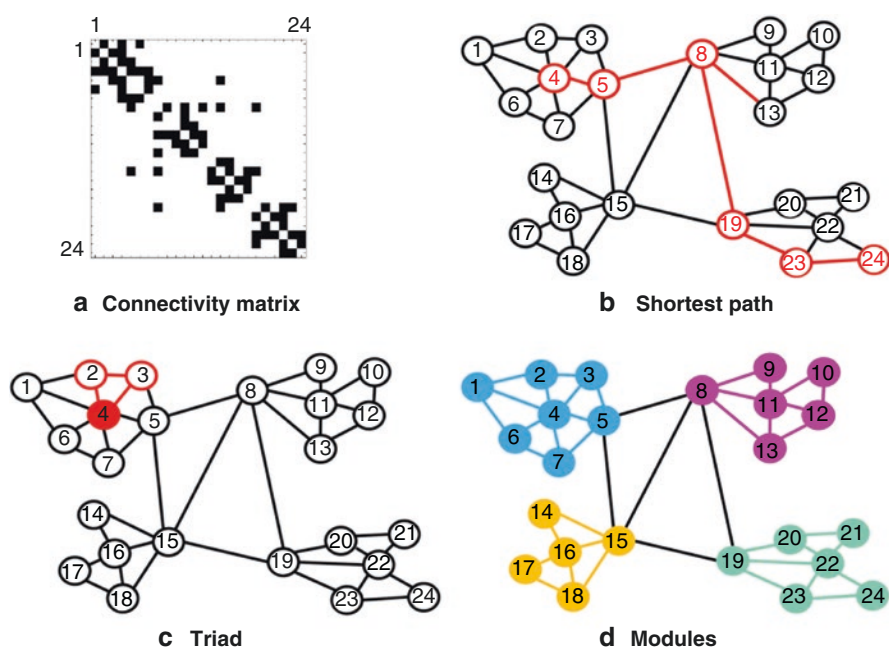


Fig. 8.4 Basics of network metrics. (a) Shows a connectivity matrix of a hypothetical network of 24 nodes. The nodes appear in order from 1 to 24 (rows or columns). Each small black square represents a binary connection between two nodes. (b–d) Display the graphic representation of the connectivity matrix, showing some fundamental topological measures (shortest path, triad and modules)

derived from Pearson's correlation coefficient) could be weak not surviving a predefined threshold. This also illustrates the idea that the formation of complex networks follows a principle of economy as stated in Sect. 3.

8.4.1 Integration

Integration metrics highlight how well-connected any pair of nodes is within the network. The topological concept of *shortest path* (Fig. 8.4b) is relevant for this concept. The shortest path is the topological distance between two nodes, for example, between nodes 4 and 24 in Fig. 8.4b. The length is the minimum number of edges between these nodes. The *path length* of a particular node (e.g., node 4) represents the shortest path of that particular node to each of the other nodes in the graph (i.e., average of *shortest path* from node 4 to node 5, node 4 to node 6, node 4 to node 7, etc.). As each node is characterized by a *path length*, the average *path length* across all nodes represents the *characteristic path length* of the network (average of path length node 4, path length node 5, path length node 6, etc.). *Path length* is a measure of nodal integration, and *characteristic path length* is a measure of network integration. A large *path length* of a node reflects a weakly connected node to the network as a whole. The opposite holds if path length is small. In this context, the definition of "large" or "small" is based on comparison with the node's path length in a reference control network (see Sect. 5 for metrics statistical comparison).

The *global efficiency* at the nodal level (also known as *nodal efficiency*) is another metric of integration. It is defined as the average of the inverse shortest path from a given node to all other nodes. Similarly, the global efficiency of the network is the *average of the global efficiency* of all nodes. The *global efficiency* (network-wide) and the *characteristic path length* are inversely related.

8.4.2 Segregation

Unlike integration measures, segregation metrics are related to how well the neighbors of a node are connected. A triad is the main concept involved with this measure (Fig. 8.4c). A triad is formed when a node is connected to any two connected neighbors. A classic measure of segregation is the nodal *clustering coefficient*, defined as the ratio between the number of triads present and the maximum number of triads that could be formed around a node. For example, the clustering coefficient of node 4 in Fig. 8.4 is 0.6 since there are 6 triads around node 4 and the maximum number of possible triads is 10 (e.g., a possible triad would be formed by the node 4 with nodes 5 and 2 if they were directly connected). The clustering coefficient can be interpreted as the probability of connection between any two neighbors of a given node. So, the *average clustering coefficient* of the network is the mean nodal clustering index across all nodes.

Another metric of segregation is the *local efficiency*. At the nodal level, it is defined as the *global efficiency* calculated on the subgraph created by the node's neighbors. Note that the concept of *global efficiency* (network-wide) defined above as a metric of integration (based on the shortest path) is used here as a metric of segregation. The difference is that the network, in this case, is only formed by the neighbors of the specific node (subnetwork or subgraph around the node) after removing it. Likewise, the *average of the local efficiency* of all nodes is the whole network level version of this metric. The *local efficiency* (network-wide) and the *average clustering coefficient* are directly related.

Modularity is a more complex segregation measure (as discussed in Sect. 2). This metric reflects the extent to which a network can be subdivided into modules (communities of nodes) with a maximal within-module and minimal between-module connectivity (Bullmore and Sporns 2009; Rubinov and Sporns 2010; Fornito et al. 2013; Garcia et al. 2018). Figure 8.4d shows in different colors the four modules that make up our hypothetical network. The modularity index Q is a network property that allows quantifying the degree of modularity of a network (Rubinov and Sporns 2010). The Q index varies from 1 to -1 . If Q index >0 and is also higher than the Q index for random networks, the network has a modular structure. To calculate the Q index, the community structure needs to be determined first. In real life, community structure detection methods are based on heuristic algorithms that result in a different partition from run to run. Therefore, to have a robust estimate of the community, the analysis requires to find a consensus partition representative of the modular structure of the network (Garcia et al. 2018).

Characteristic path length and the *average clustering coefficient* (or equivalent metrics) are usually considered the two main properties of small-world topology (introduced in Sect. 2). A metric that summarizes this is the small-worldness (also termed σ). This metric reflects to what extent a network shows an optimal balance between *characteristic path length* (integration) and *average clustering coefficient* (segregation). To assess σ , both *characteristic path length* and *average clustering coefficient* must be relative (ratio) to these identical average measures of a reference random graph. This results in λ for the *characteristic path length* and γ for the *average clustering coefficient*. σ is the ratio between γ and λ . In a complex network, σ is greater than unity because the *characteristic path length* of a complex network and a random network is expected to be similar, unlike the *average clustering coefficient* that must be greater in the complex network.

8.4.3 Centrality

The metrics of centrality measure the level of influence of a given node on other nodes in the network. The simplest measure of centrality is the *nodal degree*, defined as the number of direct connections that a node has with other nodes. For example, the nodal degree of node 4 is six because it has six direct connections to nodes 1–3 and 5–7 (Fig. 8.4b). For binary and undirected graphs, this metric is calculated as

the sum of the number of connections (black squares) across the rows or columns of the connectivity matrix (Fig. 8.4a). The *mean degree* is the average of the degrees of all nodes (network-wide degree).

The *nodal degree* version of a weighted (no binary) network is the *nodal strength*, defined as the sum of the weights of all edges connected to a node. The mean strength is the average of the strength of all nodes (network-wide strength). The *strength* (both nodal and network-wide) is useful even when using binary matrices for network metrics calculation. Before binarization, this metric serves as an exploratory step of the analysis of the dataset as it is a relatively simple measure of connectivity and less abstract than other high-order metrics. It still may be useful to normalize the *nodal strength* by the average across nodes (also known as the *strength of association*), as it is a more intuitive summary of nodal connectivity.

Another important property related to the *nodal degree (strength)* is the distribution of degree (strength) values across all nodes. The degree (strength) distribution allows to determine whether the network of interest contains hubs and to understand possible influences that they may have on the network.

Two other widely used metrics are the closeness and betweenness centralities. The first is the same metric defined above as nodal efficiency as a measure of integration, while the second is the ratio between all shortest paths that pass through the node and all shortest paths in the graph.

Two other, more complex, metrics of centrality are the *participation coefficient* and *within-module degree z-score*. Both these metrics reflect the connectivity of each node in relation to the modular organization of the brain. The participation coefficient is defined as the ratio between the number of connections that the node has outside its module (intermodular) and the total number of connections in the whole network. For example, nodes 5, 8, 15 and 19 in Fig. 8.4 have a high participation coefficient compared to other nodes, since they have intermodular connections. The within-module degree *z-score* for a given node is the nodal degree (as defined above), but restricted to only connections inside the module to which that node belongs. For example, nodes 4, 11, 16 and 22 in Fig. 8.4 have a high within-module degree *z-score* compared to other nodes.

These two last metrics provide a more appropriate way to identify the presence of hubs in correlation-based network analyses (Power et al. 2013). For instance, connector hubs have a high participation coefficient and relative high within-module degree *z-score* (nodes 5, 8, 15 and 19 in Fig. 8.4). Connector hubs have a fundamental role in network integration, and they are important in network resilience. So-called “provincial” hubs have low participation coefficient but high within-module degree *z-score* (nodes 4, 11, 16 and 22 in Fig. 8.4). Provincial hubs are fundamental in network segregation.

To identify connector hubs and provincial hubs, the modular structure of the network must first be determined. Thus, modularity is not just a segregation metric, it interrelates segregation, integration, and centrality metrics. Modularity is a key integrative concept in complex network metrics.

Detailed mathematical definitions of network metrics can be found elsewhere (Rubinov and Sporns 2010). Open-source software is readily available on

multiple websites to calculate graph metrics and perform brain connectivity analysis (e.g., (Melie-García et al. 2010; Hosseini et al. 2012; Mijalkov et al. 2017).).

8.5 Brain Connectivity Analysis

Connectivity analysis is generally performed by a statistical comparison of metrics of at least two networks. For example, comparison of network integrity of patients with a specific CNS disorder to a group of control subjects, or longitudinal assessment of network changes within a single group.

Data resampling allows for statistical comparison of network metrics (based on the connectivity matrix) between groups (or time points). One form of resampling uses a non-parametric permutation test. In this procedure: (1) ROI data of each subject are randomly reassigned (a “permutation”) to one of the two groups such that each randomized group has the same number of participants as the original ones (typically 1000 permutations or more); (2) the connectivity matrix is calculated for each randomized group; (3) binary connectivity matrices at different network densities (range of densities) are obtained by applying thresholds (as described in Sect. 3); (4) network metrics are estimated for all networks (from randomized groups) in each density; (5) differences in network metrics between randomized groups, in each density, are obtained resulting in a permutation distribution of the difference under the null hypothesis; (6) the real difference between groups in network metrics (for each density) is placed in the corresponding permutation distribution and a p -value of two tails is calculated based on its percentile position. As a critical value, the 95% confidence interval of each network metric distribution is usually considered (two-tailed test of the null hypothesis at $p < 0.05$).

Another form of resampling is by generating bootstrap samples from both networks. Normally statistical inference is based on sampling distributions of sample statistics. The bootstrap method is a way to find the sampling distribution, at least approximately, of a single sample. Therefore, the sample must represent the population from which it was extracted. In our particular case, for each of the two groups (networks), new samples (1000 or more), called bootstrap samples or resamples, are created by sampling with replacement from the original random sample (each resample is the same size as the original sample). Replacement means that after randomly drawing one observation from the original sample, we replace it before drawing the next observation, that results in two randomized groups. From here, the method follows the **steps 2–6** as described above for the permutation test. The main difference between the two procedures is in how the randomized groups are created. It is important to emphasize that in the case of the bootstrap method, the original sample should represent the population at large.

It is also important to control for multiple comparisons when comparing network metrics at the nodal level. Typically, the false discovery rate correction (FDR) procedure is used for this purpose (Benjamini and Hochberg 1995).

8.6 Sparse Inverse Covariance Estimation (SICE)

As discussed earlier, using partial correlation is the preferred method to build the connectivity matrix. The estimation of partial correlations is usually achieved by the maximum likelihood estimation (MLE) of the inverse covariance matrix, but for that estimate to be reliable, the number of subjects must be greater than the number of ROIs. Huang et al. (2010) introduced the idea of analyzing brain metabolic connectivity based on FDG-PET using so-called graphical lasso, in which a constraint imposed on MLE allows for estimation of the inverse covariance matrix even when the number of subjects is less than the number of ROIs (Huang et al. 2010). The connectivity matrix estimated by this approach is binary (1 = connection, 0 = no connection). Instead of the exact value of the nonzero entries in the inverse covariance matrix, this methodology discovers the zero entries (i.e., no connection) by using a regularization parameter (known as λ ; not related to the small worldness metric) that controls the zero entries number in the connectivity matrix. The λ parameter controls a trade-off between the likelihood fit of the inverse covariance estimation and matrix sparsity. A small λ will result in a higher likelihood fit of the inverse covariance estimation, while a large λ will result in a sparser estimation (low network density or sparsity). Since whole brain networks tend to be sparse, λ should be relatively high. Hence the name sparse inverse covariance estimation (SICE). λ , however, cannot be too high since it reduces the likelihood fit of the inverse covariance estimation. The determination of λ is a key step when using SICE although there is no gold standard for the selection of this parameter. One proposed λ selection method is Stability Approach to Regularization Selection (StARS) (Liu et al. 2010). This method selects the minimum λ necessary to capture the correct structure of the connectivity matrix and at the same time guarantees a relatively low matrix sparsity (low network density) and replicability under random sampling. An important assumption of SICE analysis is multivariate normality distribution of the data.

Since SICE matrices are also graphs, all previously described network metrics and statistical inference methods are applicable. Nevertheless, the original idea of the analysis of SICE matrices was based on submatrices and their interactions (also applicable to any other type of connectivity matrix). The submatrix based approach involves subdividing the connectivity matrix into smaller submatrices. For example, Huang et al. (Huang et al. 2010) made this subdivision based on 42 ROIs of cerebral regions to be the most affected by Alzheimer disease (AD), as revealed by FDG-PET (Horwitz et al. 1984). These ROIs were then distributed in four submatrices representing ROIs of the frontal, parietal, occipital, and temporal lobes successively (Fig. 8.5). The submatrix based analysis consists of calculating the total number of connections within a submatrix (number of black dots within red squares in Fig. 8.5) and the total number of connections between two submatrices. The total number of connections within a submatrix represents the “short distance” connections, while between two submatrices they represent the “long distance” connections (i.e., the interaction between two submatrices). For instance, in Fig. 8.5, the connections within the temporal lobe are decreased in the matrix representing the AD group

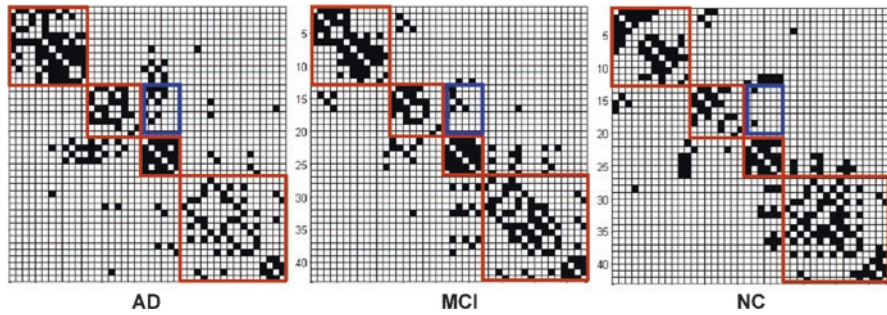


Fig. 8.5 Brain connectivity models using SICE. The figure shows the model for AD dementia, MCI and normal control (NC) subjects. The red squares, from top left to bottom right, represent the ROIs of the frontal, parietal, occipital, and temporal lobes. The blue square represents the interaction between the parietal and occipital lobes. (Image adapted from Huang et al. (2010))

compared to the control group, while they are increased between the parietal and occipital lobes (blue squares).

In addition, Huang et al. (2010) showed a monotonous property of SICE, which allowed them to develop a quasi-measure for the strength of functional connections. The monotonous property of SICE states that if two regions of the brain are not connected at a certain λ , they will never be connected as λ becomes larger. Recent articles used this concept (e.g., see (Caminiti et al. 2017; Sala et al. 2017)).

8.7 Example Studies

In this section, findings of selected articles are briefly described to illustrate the concepts explained in previous sections.

8.7.1 Age-Associated Metabolic Network Changes

This example highlights the utility of *characteristic path length* and *average clustering coefficient* (main properties of small-world topology) as well as the *betweenness* centrality. Liu et al. (2014) investigated whether small-world topology of the brain metabolic network changes with aging (Liu et al. 2014). The authors built two brain networks based on FDG-PET using partial correlation: one from healthy young adults (mean age = 36.5 years, 113 individuals) and the other from healthy older adults (mean age = 56.3 years, 110 individuals). The connectivity matrices associated with each group were binarized and the statistical differences were assessed using a non-parametric permutation test in a range of network density (sparsity) between 10% and 50%. They found that networks from both young and old adults showed small-world topologies. However, the *characteristic path length* and the *average clustering coefficient* were increased in the older group compared to the younger group (Figs. 8.6 and 8.7, respectively).

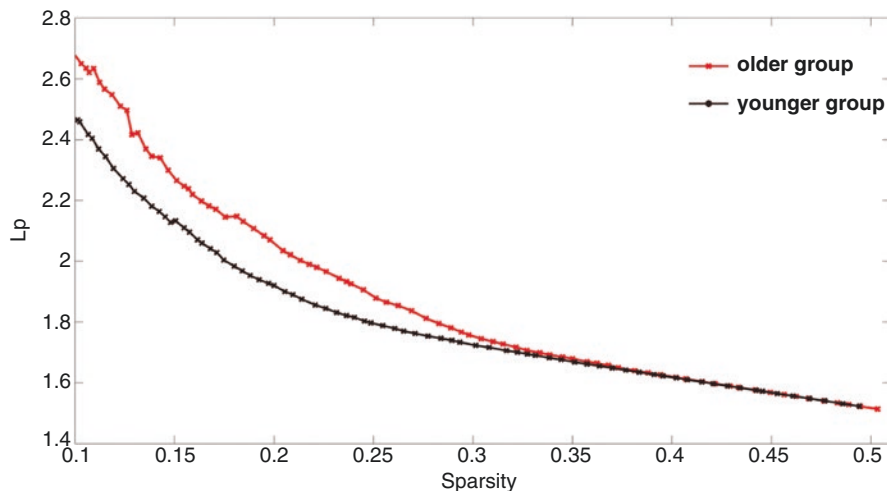


Fig. 8.6 The *characteristic path length* (L_p) as a function of sparsity (S). The graph shows that two groups have same L_p value when sparsity ranges from 33% to 50% and the older group (red line) has larger L_p at $10\% < S < 33\%$. (Image reproduced from Liu et al. (2014))

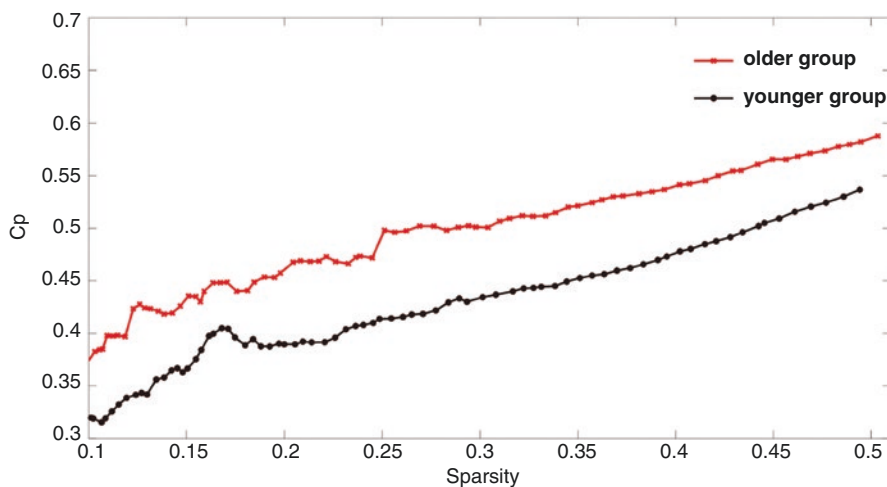


Fig. 8.7 The *average clustering coefficient* (C_p) as a function of sparsity (S). The graph shows that, at a wide range of sparsity ($10\% < S < 50\%$), the older subjects (red line) have larger C_p values than the younger subjects (black line). (Image reproduced from Liu et al. (2014))

Liu et al. (2014) also analyzed *nodal centrality* using the *betweenness*. They found that the younger group showed higher *betweenness* in the hippocampus and auditory cortex on the left side, and the amygdala and superior frontal gyrus on the right side. In contrast, the older group showed higher *betweenness* in the orbital frontal cortex bilaterally and the right insula (Fig. 8.8).

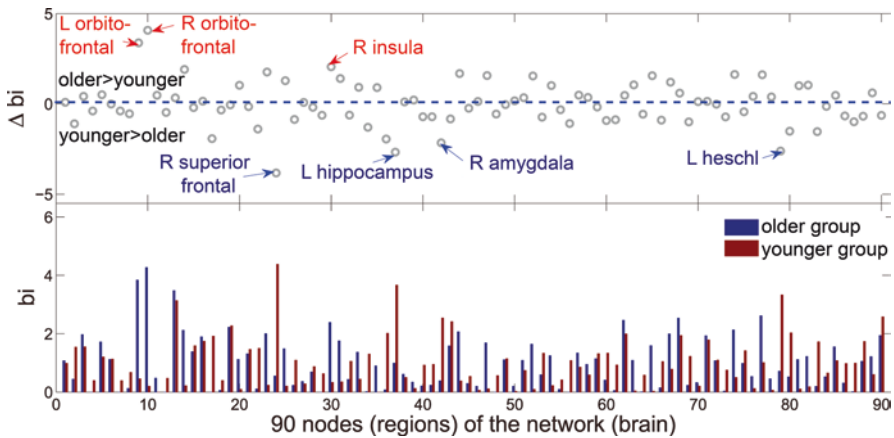


Fig. 8.8 The betweenness centrality (bi) of the two groups. The upper graph shows the regional changes (Δbi , $\Delta bi = bi_{older} - bi_{younger}$) between the two groups. The regions labeled in the upper graph indicate significant bi changes. These results were obtained from a network density of 16%. (Images adapted from Liu et al. (2014))

Similar results with respect to the *characteristic path length* have also been found when comparing age-matched controls with patients with mild cognitive impairment (MCI) and AD in network analyses based on FDG-PET (Sanabria-Diaz et al. 2013) and perfusion SPECT (Sanchez-Catasus et al. 2018), in both cases using simple correlation matrices. The increase of the *characteristic path length* was interpreted as a result of loss of brain connectivity due to AD pathology. Findings of these studies suggest that brain changes, whether age-associated or associated with cognitive change, can be adequately captured by network metrics based on FDG-PET and perfusion SPECT. Both age- and cognition-associated brain changes have a perceptible effect on the topology of the brain metabolic network.

8.7.2 Modularity of Amyloid Networks

In this example, we will focus on the utility of modularity analysis. Pereira et al. (2018) analyzed the topology of the amyloid network in non-demented individuals in different stages of $A\beta$ accumulation (Pereira et al. 2018). The authors analyzed three groups of subjects according to $A\beta_{42}$ levels in the cerebro-spinal fluid (CSF) and Florbetapir β -amyloid PET biomarkers (CSF-/PET-, $n = 291$; CSF+/PET-, $n = 81$; and CSF+/PET+, $n = 272$). PET-based β -amyloid networks were created using partial correlation (Figs. 8.9a, b).

Similar to the previously described study by Liu et al. (2014), they use binary matrices and non-parametric permutation test in a range of network densities between 5% and 15%. They performed a modularity analysis and used several network metrics at the nodal level. Two modules were identified that were present in the three groups (Fig. 8.10). One of these modules comprised several regions that

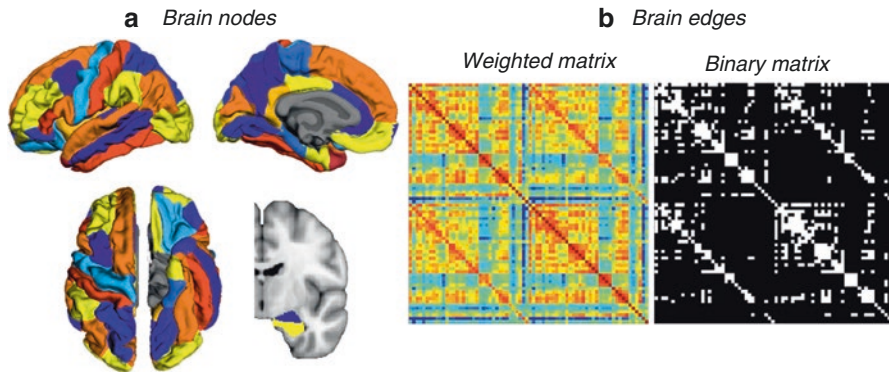


Fig. 8.9 (a) Brain parcellation (72 ROIs). (b) Weighted and binary matrices (*Image reproduced from Pereira et al. (2018)*)

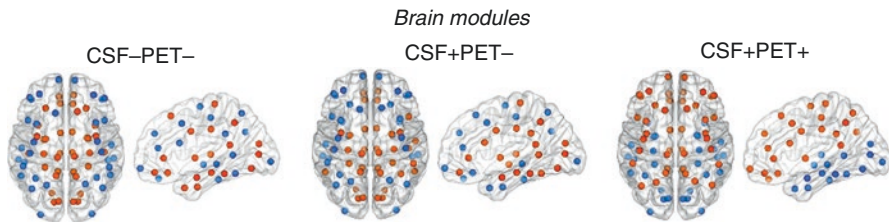


Fig. 8.10 The two modules identified in the three groups studied. The spheres represent the nodes belonging to each module (orange and blue colors). (*Image reproduced from Pereira et al. (2018)*)

are part of the default mode network (anterior cingulate, posterior cingulate and precuneus) but also included additional lateral temporal and parietal areas in the CSF + PET– group and lateral frontal in the CSF + PET+ group. These findings are in line with the current pathological knowledge of spread of β -amyloid pathology with progression to AD dementia (Braak and Braak 1991). This suggests that analysis of the topology of the amyloid network could potentially be used to assess disease progression in stages prior to dementia.

8.7.3 Cerebrovascular Reactivity in MCI

This example will highlight the complementary role of network analysis in interpreting univariate analysis results. Sanchez-Catusus et al. (2017) examined cerebrovascular reactivity (CVR) in MCI and healthy conditions by analyzing vasodilator-induced changes in the topology of the CBF network (Sanchez-Catusus et al. 2017). For this purpose, four networks were constructed (based on simple correlation): two using CBF SPECT data at baseline and under the vasodilatory challenge of acetazolamide (ACZ) corresponding to 26 MCI patients and two equivalent networks from 26 matching cognitively normal controls. The strength of association

and the clustering coefficient were used as network metrics (network-wide and nodal). The data were analyzed by a 2 (group: Control and MCI) \times 2 (condition: basal and ACZ) design. Simple main effects and their interactions were statistically determined using the bootstrap resampling approach. A 2 \times 2 design was also used for voxel-based univariate analysis. In addition, voxel-based univariate analysis of MRI data was carried out. Results showed no significant differences between groups in response to the ACZ challenge by the univariate approach. In contrast, the network analysis showed different patterns of changes in the strength of association and clustering coefficient (network-wide and nodal). However, the most striking finding was the crossover interaction between group and condition found in the network analysis, particularly for the nodal clustering coefficient (Fig. 8.11a). This interaction effect showed a pattern of decrease of the *clustering coefficient* in the MCI group that partially overlapped with the default mode network, which is a target of AD-like neurodegenerative process. Surprisingly, this pattern also partially corresponded with the regional CBF reduction found in the MCI group in the baseline condition (Fig. 8.11b). The overlap increases if the atrophy found by MRI analysis is considered (Fig. 8.11c), suggesting that the functional and structural abnormalities found by the univariate approach in the baseline condition could explain the ACZ-induced changes found by the graph theoretical analysis. In this example, both multivariate and univariate analysis approaches provided complementary information that led to a more comprehensive understanding of CVR in MCI.

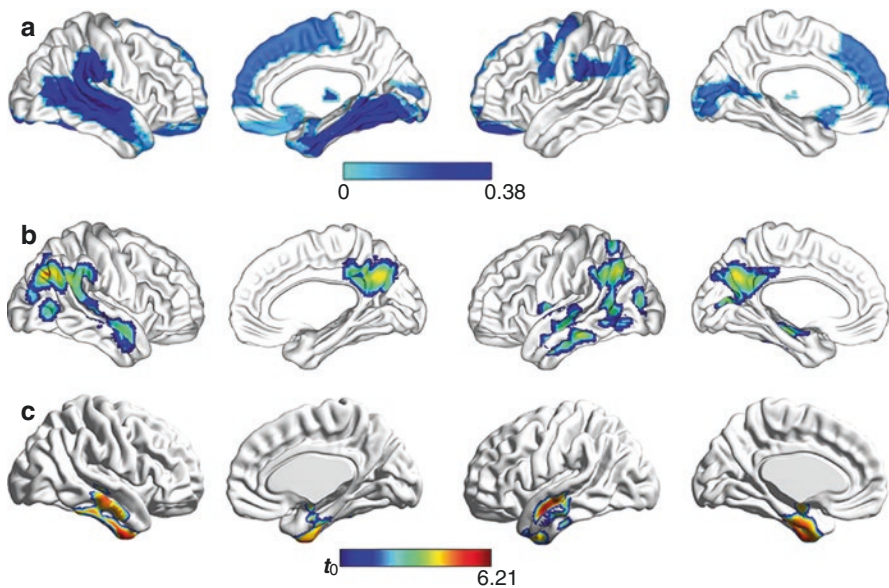


Fig. 8.11 (a) Decrease of the clustering coefficient in the MCI group network induced by the vasodilatory challenge (crossover interaction between group and condition); (b) hypoperfusion in the MCI group in the baseline condition; and (c) atrophy in the MCI group. (Images adapted from Sanchez-Catasus et al. (2017))

8.7.4 SICE Application to Multimodal Neuroimaging

This example will highlight the versatility of SICE analysis. Li et al. (2018) compared networks of patients with AD ($n = 116$; 64 m/52f) and MCI ($n = 116$; 64 m/52 f) to networks constructed with normal subjects ($n = 116$; 62 m/54 f), based on structural MRI, FDG-PET and Florbetapir β -amyloid PET (Li et al. 2018). The authors used the SICE methodology to create connectivity matrices for each group that included the three image modalities. The authors used the same ROIs as Huang et al. (2010), excluding frontal ROIs (see Sect. 6). For illustrative purposes results are only discussed for one of the multimodal connectivity models. The models presented in Fig. 8.12 demonstrate how network connectivity can be applied to a single modality but also the interaction between modalities (e.g., interactions of the β -amyloid network with the metabolic or with a network based on structural brain volumes). The figure shows a gradient of decreasing number of connections (black dots) within modalities from control to MCI and then to AD dementia, while the interaction between modalities gradually increased between these groups. This analysis would be impossible using simple correlation connectivity matrices and the partial correlation option would have required a very large sample of data, with a prohibitive cost in PET studies.

8.8 Final Remarks

The network analysis methods described in this chapter provide a powerful tool for a better understanding of metabolic, perfusion, neurotransmitter, and neuropathological brain changes, particularly in the context of aging and neurodegenerative diseases. These multivariate methods allow for analysis of the neuroimaging data and subsequent results that could be missed when a univariate brain region or even voxel-based whole brain analysis is used. Both approaches, however, are complementary, and simultaneous analysis and interpretation provide a higher level of understanding of brain function than either one alone.

The abundance of metrics that graph analysis of network properties provides allows for a detailed description of network properties. For example, nuclear medicine neuroimaging-based connectivity studies commonly use the main properties of small-world topology, i.e., the characteristic path length and average clustering coefficient (or equivalent network-wide or local metrics). This level of analysis characterizes networks within the spectrum from random to regular (ordered) topologies. Other commonly used graph analysis metrics involve centrality metrics, which allow the identification of hubs, but without distinction between connectors and provincial hubs. We emphasize that modularity analysis is important to take into account, as it offers an integrative analysis of complex network metrics, properly defining, for example, connectors and provincial hubs.

The plethora of graph analysis metrics to choose from poses also a challenge in selecting the appropriate measures. A first consideration to be made in the selection

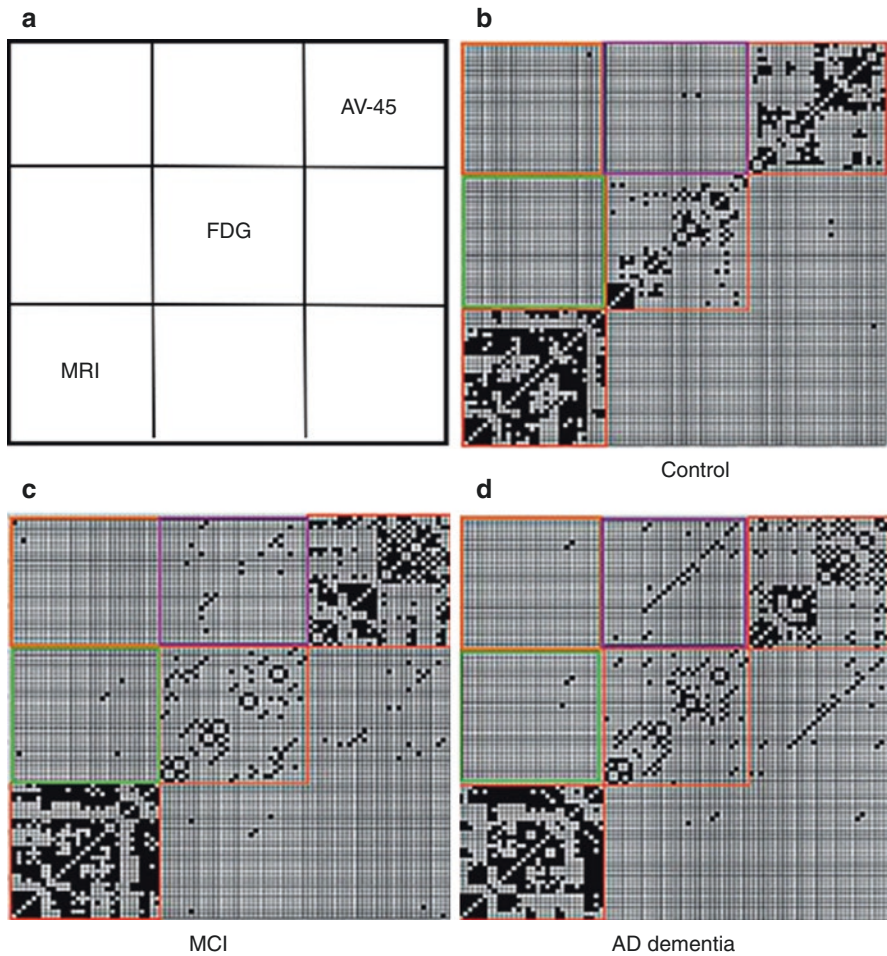


Fig. 8.12 Brain connectivity models using SICE based on multimodal data. (a) Matrix indicative of the subdivision into submatrices (30×30 ROIs) of the data corresponding to AV-45 (Florbetapir-PET), FDG-PET, and MRI (brain volumes). The figure shows the model for normal control (b), MCI (c), and AD dementia (d). (Images adapted from Li et al. (2018))

of one of these two methods is whether complex multivariate approaches are justified or if the specific scientific question can be solved with univariate methodology. A second consideration is to properly select those metrics that will address the a priori scientific hypothesis. A final consideration, which is especially important for nuclear molecular neuroimaging studies, is whether network analysis adequately reflects the underlying biology, for example, known neurotransmitter distribution and/or neuropathology. Network analysis of radiotracers with limited specificity will inherently be noisier. However, this problem exists also in univariate analysis approaches.

The study of brain molecular connectivity using nuclear medicine neuroimaging has gradually matured, but there are many remaining challenges. Solving such challenges will offer new opportunities to expand our knowledge of molecular brain networks. A multimodal approach using complementary network information from both MRI and nuclear molecular imaging will ultimately provide a more comprehensive insight into brain network functioning. PET and SPECT brain network analysis tools are now able to overcome limitations of standard univariate approach in neuro-nuclear medicine. We anticipate that molecular brain network analysis may become part of clinical nuclear medicine practice in the near future.

A Lexicon of the Most Commonly Used Network Metrics

- **Shortest path:** Topological distance between two nodes, also called *Length*, as the minimum number of edges between two nodes.
- **Path length:** Shortest path of a given node to each of the other nodes.
- **Characteristic path length:** Average path length node across all nodes.
- **Global efficiency:** Average of the inverse shortest path from a given node to all other nodes. At the network level, it is the average of the global efficiency of all nodes.
- **Triad:** Formed when a node is connected to any two connected neighbors.
- **Clustering coefficient:** The ratio between the number of triads present around a node and the maximum number of triads that could be formed around that node. At the network level, it is the average of the clustering coefficient of all nodes.
- **Local efficiency (nodal level):** The global efficiency calculated on the subgraph created by the node's neighbors. At the network level, it is the average of the local efficiency of all nodes.
- **Modularity:** The extent to which a network can be subdivided into modules (communities of nodes) with a maximal within-module and minimal between-module connectivity.
- **The small-worldness (σ):** The extent to which a network shows an optimal balance between *characteristic path length* (integration) and *average clustering coefficient* (segregation).
- **Degree:** The number of direct connections that a node has with other nodes. At the network level, it is the average of the degrees of all nodes.
- **Strength:** The sum of the weights of all edges connected to a node. At the network level, it is the average of the strength of all nodes.
- **Closeness centrality:** The same as the global efficiency at the nodal level.
- **Betweenness centrality:** The ratio between all shortest paths that pass through the node and all shortest paths in the graph.
- **Participation coefficient:** The ratio between the number of connections that the node has outside its module (intermodular) and the total number of connections in the whole network.
- **Within-module degree z-score:** The nodal degree but restricted to only connections inside the module to which that node belongs.

References

- Anticevic A, Cole MW, Murray JD, Corlett PR, Wang XJ, Krystal JH (2012) The role of default network deactivation in cognition and disease. *Trends Cogn Sci* 16(12):584–592
- Bassett DS, Bullmore ET (2017) Small-world brain networks revisited. *Neuroscientist* 23(5):499–516
- Batalle D, Munoz-Moreno E, Figueras F, Bargallo N, Eixarch E, Gratacos E (2013) Normalization of similarity-based individual brain networks from gray matter MRI and its association with neurodevelopment in infants with intrauterine growth restriction. *NeuroImage* 83:901–911
- Benjamini Y, Hochberg Y (1995) Controlling the false discovery rate: a practical and powerful approach to multiple testing. *J R Stat Soc Series B* 1:289–300
- Biggs N, Lloyd E, Wilson R (1986) *Graph theory*. Oxford University Press, Oxford, pp 1736–1936
- Braak H, Braak E (1991) Neuropathological staging of Alzheimer-related changes. *Acta Neuropathol* 82(4):239–259
- Bullmore E, Sporns O (2009) Complex brain networks: graph theoretical analysis of structural and functional systems. *Nat Rev Neurosci* 10(3):186–198
- Bullmore E, Sporns O (2012) The economy of brain network organization. *Nat Rev Neurosci* 13(5):336–349
- Caminiti SP, Tettamanti M, Sala A, Presotto L, Iannaccone S, Cappa SF et al (2017) Metabolic connectomics targeting brain pathology in dementia with Lewy bodies. *J Cereb Blood Flow Metab* 37(4):1311–1325
- Clark CM, Stoessl AJ (1986) Glucose use correlations: a matter of inference. *J Cereb Blood Flow Metab* 6(4):511–512
- David O, Guillemain I, Saittel S, Reyt S, Deransart C, Segebarth C et al (2008) Identifying neural drivers with functional MRI: an electrophysiological validation. *PLoS Biol* 6(12):2683–2697
- Eidelberg D, Moeller JR, Dhawan V, Spetsieris P, Takikawa S, Ishikawa T et al (1994) The metabolic topography of parkinsonism. *J Cereb Blood Flow Metab* 14(5):783–801
- Fornito A, Bullmore ET (2015) Connectomics: a new paradigm for understanding brain disease. *Eur Neuropsychopharmacol* 25(5):733–748
- Fornito A, Zalesky A, Breakspear M (2013) Graph analysis of the human connectome: promise, progress, and pitfalls. *NeuroImage* 80:426–444
- Friston KJ (2011) Functional and effective connectivity: a review. *Brain Connect* 1(1):13–36
- Garcia JO, Ashourvan A, Muldoon SF, Vettel JM, Bassett DS (2018) Applications of community detection techniques to brain graphs: algorithmic considerations and implications for neural function. *Proc IEEE Inst Electr Electron Eng* 106(5):846–867
- Gu SC, Ye Q, Yuan CX (2019) Metabolic pattern analysis of 18F-FDG PET as a marker for Parkinson's disease: a systematic review and meta-analysis. *Rev Neurosci*
- Hahn A, Lanzenberger R, Kasper S (2019) Making sense of connectivity. *Int J Neuropsychopharmacol* 22(3):194–207
- Honey CJ, Thivierge JP, Sporns O (2010) Can structure predict function in the human brain? *NeuroImage* 52(3):766–776
- Horwitz B, Duara R, Rapoport SI (1984) Intercorrelations of glucose metabolic rates between brain regions: application to healthy males in a state of reduced sensory input. *J Cereb Blood Flow Metab* 4(4):484–499
- Horwitz B, Grady CL, Schlageter NL, Duara R, Rapoport SI (1987) Intercorrelations of regional cerebral glucose metabolic rates in Alzheimer's disease. *Brain Res* 407(2):294–306
- Hosseini SM, Hoefl F, Kesler SR (2012) GAT: a graph-theoretical analysis toolbox for analyzing between-group differences in large-scale structural and functional brain networks. *PLoS One* 7(7):e40709
- Huang S, Li J, Sun L, Ye J, Fleisher A, Wu T et al (2010) Learning brain connectivity of Alzheimer's disease by sparse inverse covariance estimation. *NeuroImage* 50(3):935–949
- Koch MA, Norris DG, Hund-Georgiadis M (2002) An investigation of functional and anatomical connectivity using magnetic resonance imaging. *NeuroImage* 16(1):241–250

- Lee DS, Kang H, Kim H, Park H, Oh JS, Lee JS et al (2008) Metabolic connectivity by inter-regional correlation analysis using statistical parametric mapping (SPM) and FDG brain PET; methodological development and patterns of metabolic connectivity in adults. *Eur J Nucl Med Mol Imaging* 35(9):1681–1691
- Li Q, Wu X, Xie F, Chen K, Yao L, Zhang J et al (2018) Aberrant connectivity in mild cognitive impairment and Alzheimer disease revealed by multimodal neuroimaging data. *Neurodegener Dis* 18(1):5–18
- Liu H, Roeder K, Wasserman L (2010) Stability approach to regularization selection (StARS) for high dimensional graphical models. *Adv Neural Inf Process Syst* 24:1432–1440
- Liu Z, Ke L, Liu H, Huang W, Hu Z (2014) Changes in topological organization of functional PET brain network with normal aging. *PLoS One* 9(2):e88690
- Manzanera OM, Meles SK, Leenders KL, Renken RJ, Pagani M, Arnaldi D et al (2019) Scaled subprofile modeling and convolutional neural networks for the identification of Parkinson's disease in 3D nuclear imaging data. *Int J Neural Syst* 1950010
- Melie-García L, Sanabria-Diaz G, Iturria-Medina Y, Alemán-Gómez Y (2010) MorphoConnect: toolbox for studying structural brain networks using morphometric descriptors. In: 16th annual meeting of the Organization for Human Brain Mapping. Human Brain Mapping (HBM), Barcelona
- Melie-García L, Sanabria-Diaz G, Sanchez-Catasus C (2013) Studying the topological organization of the cerebral blood flow fluctuations in resting state. *NeuroImage* 64:173–184
- Metter EJ, Riege WH, Kuhl DE, Phelps ME (1984) Cerebral metabolic relationships for selected brain regions in healthy adults. *J Cereb Blood Flow Metab* 4(1):1–7
- Mijalkov M, Kakaei E, Pereira JB, Westman E, Volpe G (2017) BRAPH: a graph theory software for the analysis of brain connectivity. *PLoS One* 12(8):e0178798
- Mišić B, Betzel RF, de Reus MA, van den Heuvel MP, Berman MG, McIntosh AR et al (2016) Network-level structure-function relationships in human neocortex. *Cereb Cortex* 26(7):3285–3296
- Moeller JR, Strother SC, Sidtis JJ, Rottenberg DA (1987) Scaled subprofile model: a statistical approach to the analysis of functional patterns in positron emission tomographic data. *J Cereb Blood Flow Metab* 7(5):649–658
- Monakow C (1914) Die Lokalisation im Grosshirn und der Abbau der Funktion durch Kortikale Herde. J. F. Bergman, Wiesbaden, pp 26–34
- Murphy K, Fox MD (2017) Towards a consensus regarding global signal regression for resting state functional connectivity MRI. *NeuroImage* 154:169–173
- Murphy K, Birn RM, Handwerker DA, Jones TB, Bandettini PA (2009) The impact of global signal regression on resting state correlations: are anti-correlated networks introduced? *NeuroImage* 44(3):893–905
- Passow S, Specht K, Adamsen TC, Biermann M, Brekke N, Craven AR et al (2015) Default-mode network functional connectivity is closely related to metabolic activity. *Hum Brain Mapp* 36(6):2027–2038
- Pereira JB, Strandberg TO, Palmqvist S, Volpe G, van Westen D, Westman E et al (2018) Amyloid network topology characterizes the progression of Alzheimer's disease during the Predementia stages. *Cereb Cortex* 28(1):340–349
- Power JD, Schlaggar BL, Lessov-Schlaggar CN, Petersen SE (2013) Evidence for hubs in human functional brain networks. *Neuron* 79(4):798–813
- Raj A, Mueller SG, Young K, Laxer KD, Weiner M (2010) Network-level analysis of cortical thickness of the epileptic brain. *NeuroImage* 52(4):1302–1313
- Riedl V, Utz L, Castrillón G, Grimmer T, Rauschecker JP, Ploner M et al (2016) Metabolic connectivity mapping reveals effective connectivity in the resting human brain. *Proc Natl Acad Sci U S A* 113(2):428–433
- Rubinov M, Sporns O (2010) Complex network measures of brain connectivity: uses and interpretations. *NeuroImage* 52(3):1059–1069
- Saad ZS, Gotts SJ, Murphy K, Chen G, Jo HJ, Martin A et al (2012) Trouble at rest: how correlation patterns and group differences become distorted after global signal regression. *Brain Connect* 2(1):25–32

- Saggar M, Hosseini SM, Bruno JL, Quintin EM, Raman MM, Kesler SR et al (2015) Estimating individual contribution from group-based structural correlation networks. *NeuroImage* 120:274–284
- Sala A, Perani D (2019) Brain molecular connectivity in neurodegenerative diseases: recent advances and new perspectives using positron emission tomography. *Front Neurosci* 13:617
- Sala A, Caminiti SP, Presotto L, Premi E, Pilotto A, Turrone R et al (2017) Altered brain metabolic connectivity at multiscale level in early Parkinson's disease. *Sci Rep* 7(1):4256
- Sanabria-Diaz G, Martinez-Montes E, Melie-Garcia L (2013) Glucose metabolism during resting state reveals abnormal brain networks organization in the Alzheimer's disease and mild cognitive impairment. *PLoS One* 8(7):e68860
- Sanchez-Catasus CA, Sanabria-Diaz G, Willemsen A, Martinez-Montes E, Samper-Noa J, Aguila-Ruiz A et al (2017) Subtle alterations in cerebrovascular reactivity in mild cognitive impairment detected by graph theoretical analysis and not by the standard approach. *Neuroimage Clin* 15:151–160
- Sanchez-Catasus CA, Willemsen A, Boellaard R, Juarez-Orozco LE, Samper-Noa J, Aguila-Ruiz A et al (2018) Episodic memory in mild cognitive impairment inversely correlates with the global modularity of the cerebral blood flow network. *Psychiatry Res Neuroimaging* 282:73–81
- Sepulcre J, Sabuncu MR, Becker A, Sperling R, Johnson KA (2013) In vivo characterization of the early states of the amyloid-beta network. *Brain* 136(Pt 7):2239–2252
- Skudlarski P, Jagannathan K, Calhoun VD, Hampson M, Skudlarska BA, Pearlson G (2008) Measuring brain connectivity: diffusion tensor imaging validates resting state temporal correlations. *NeuroImage* 43(3):554–561
- Sporns O, Tononi G, Kötter R (2005) The human connectome: a structural description of the human brain. *PLoS Comput Biol* 1(4):e42
- Tijms BM, Series P, Willshaw DJ, Lawrie SM (2012) Similarity-based extraction of individual networks from gray matter MRI scans. *Cereb Cortex* 22(7):1530–1541
- Titov D, Diehl-Schmid J, Shi K, Pernecky R, Zou N, Grimmer T et al (2017) Metabolic connectivity for differential diagnosis of dementing disorders. *J Cereb Blood Flow Metab* 37(1):252–262
- Tomasi DG, Shokri-Kojori E, Wiers CE, Kim SW, Demiral SB, Cabrera EA et al (2017) Dynamic brain glucose metabolism identifies anti-correlated cortical-cerebellar networks at rest. *J Cereb Blood Flow Metab* 37(12):3659–3670
- Tzourio-Mazoyer N, Landeau B, Papathanassiou D, Crivello F, Etard O, Delcroix N et al (2002) Automated anatomical labeling of activations in SPM using a macroscopic anatomical parcellation of the MNI MRI single-subject brain. *NeuroImage* 15(1):273–289
- Veronese M, Moro L, Arcolin M, Dipasquale O, Rizzo G, Expert P et al (2019) Covariance statistics and network analysis of brain PET imaging studies. *Sci Rep* 9(1):2496
- Watts DJ, Strogatz SH (1998) Collective dynamics of 'small-world' networks. *Nature* 393(6684):440–442
- Yakushev I, Drzezga A, Habeck C (2017) Metabolic connectivity: methods and applications. *Curr Opin Neurol* 30(6):677–685
- Zhou L, Wang Y, Li Y, Yap PT, Shen D (2011) Hierarchical anatomical brain networks for MCI prediction: revisiting volumetric measures. *PLoS One* 6(7):e21935